

## 11B.4 Improving the Detection Probability of Low Clutter-to-Signal Ratio Ground Clutter Contamination in the WSR-88D

Scott Ellis\*; and G. Meymaris\*, J. C. Hubbert\*, M. J. Dixon\*, G. T. McGehee\*\*, J. C. Krause\*\*, and R. L. Ice\*\*

\*NCAR, Boulder, CO

\*\*Radar Operations Center, Norman OK

### 1 Introduction

The CMD algorithm has been shown to identify clutter mixed with weather in many circumstances and the results are generally good for Z and Vr. However CMD cannot detect clutter underlying weather echoes with very low CSR values resulting in the 'clutter footprint' issue. This section provides a brief background on the clutter footprint and its causes.

#### 1.1 The sensitivity of different dual-pol variables to low CSR clutter

The dual-polarmetric variables,  $\rho_{HV}$ ,  $Z_{dr}$  and  $\Phi_{DP}$ , are much more sensitive to the presence of underlying clutter than Z, Vr and SW. The  $\rho_{HV}$ ,  $Z_{dr}$  and  $\Phi_{DP}$  can suffer significant bias even in the case when the clutter echo has much less power than the overlaid weather echo. This makes sense because these variable are differential quantities that measure small differences between large quantities. Therefore small errors in either H or V power and phase can result in substantial errors in  $\rho_{HV}$ ,  $Z_{dr}$  and  $\Phi_{DP}$ . This was demonstrated by Friedrich et al. (2009), who showed that  $\rho_{HV}$ ,  $Z_{dr}$  and  $\Phi_{DP}$  obtain unacceptably large biases at much lower CSR clutter than Z and Vr. The magnitude of the errors incurred were also found to be sensitive to the characteristics of the clutter and the weather echo, consistent with our previous findings (Hubbert et al. 2011). The implication is that there is not a single value of CSR for which the clutter filter should be applied to a given variable. Further, Friedrich et al. (2009) found that  $\rho_{HV}$  is the most sensitive parameter to low CSR ground clutter. Figure 1, adapted from Fig. 13 of Friedrich et al (2009) summarizes their results. Shown are the minimum values of CSR that result in data that exceed a predetermined variance thresholds that indicate high-enough quality measurements. The mean maximum CSR shown in Fig. 1 that results in acceptable  $\rho_{HV}$  is about -13 dB with a span from -18 to -7 dB.

#### 1.2 The sensitivity of different dual-pol variables to the GMAP clutter filter

Not only are dual-pol variables impacted differently by low CSR clutter, there are also differences in the impact of applying the GMAP clutter filter. Consider the data presented in Fig 2 which shows the Z and Vr from KRIW (Riverton WY) with no clutter filter applied. The 0 m/s line can be seen in Vr as the gray and tan colors. The corresponding unfiltered  $\rho_{HV}$  field is shown in Fig 3. The data shown are from a stratiform snow case and the  $\rho_{HV}$  of the snow echoes should be quite close to 1.0 (yellow) throughout the domain.

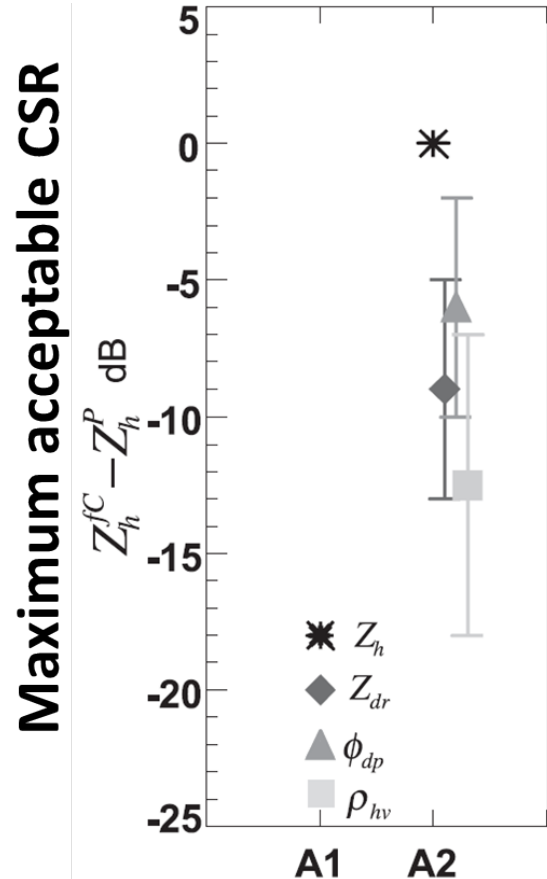


Figure 1: The maximum CSR to obtain acceptable errors in  $Z_h$  HV,  $Z_{dr}$  and DP as defined by the authors. The results are from a modeling study and are illustrative of the different sensitivity of the variables to ground clutter underlying weather echo. Adapted from Fig. 13 of Friedrich et al. (2009).

Therefore all of the low values of  $\rho_{HV}$  seen in fig 3 are biased from ground clutter mixed with weather echoes at various CSR values. Comparing unfiltered Z and  $\rho_{HV}$  their different susceptibility to low CSR clutter is apparent. Figure 4 shows the Z and  $\rho_{HV}$  after applying GMAP to all bins. Examining the Z field within the ovals in Figs 2 and 4 it can be seen that the application of GMAP introduces a large negative bias to Z in the 0 m/s isodop, as is expected. However within the same regions in the ovals the application of GMAP leads to a substantial improvement in the  $\rho_{HV}$ . This is due to GMAP removing the underlying ground clutter that caused large errors in  $\rho_{HV}$ . It is also seen that GMAP application results in biases in  $\rho_{HV}$  within the 0 m/s isodop, however the spatial extent of the biased region is much smaller than the biased region

for Z. Therefore application of GMAP in some regions can simultaneously help  $\rho_{HV}$  and hurt Z. The Zdr and  $\Phi_{DP}$  are similar in impact by GMAP as  $\rho_{HV}$  (not shown).

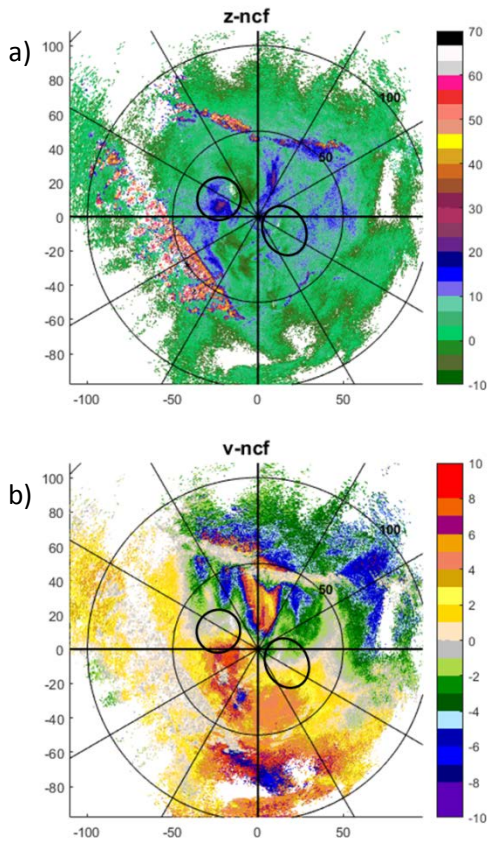


Figure 2: Z (a) and Vr (b) from KRIW with no clutter filtering applied. The data were collected on 24 January 2017 and the elevation angle is 1.5 deg.

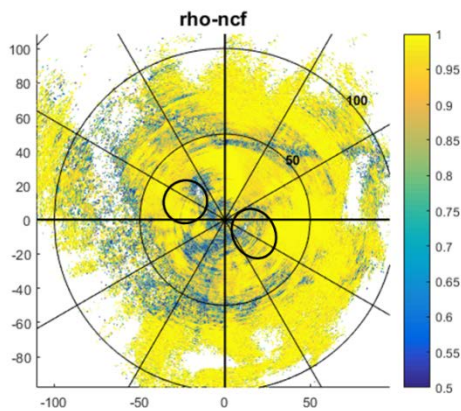


Figure 3:  $\rho_{HV}$ , from KRIW with no clutter filtering applied. The data were collected on 24 January 2017 and the elevation angle is 1.5 deg.

The different impacts of low CSR clutter on the different radar fields described in Section 1.1

combined with the different sensitivity of the fields to the application of GMAP described above suggests different clutter filter regions for different radar fields. For example, in a low CSR region, the resulting errors in Z and Vr may be quite small, but the errors in  $\rho_{HV}$ , Zdr and  $\Phi_{DP}$  can be quite large. In this region applying GMAP would be beneficial to  $\rho_{HV}$ , Zdr and  $\Phi_{DP}$  but could cause large errors in Z and Vr.

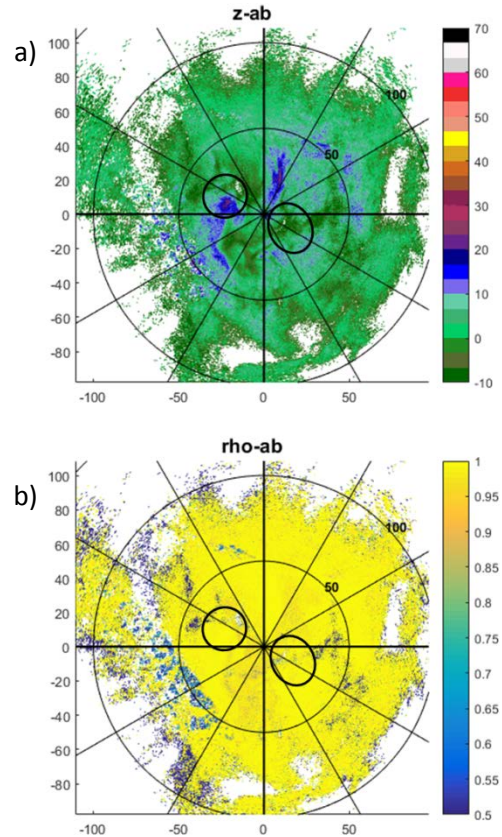
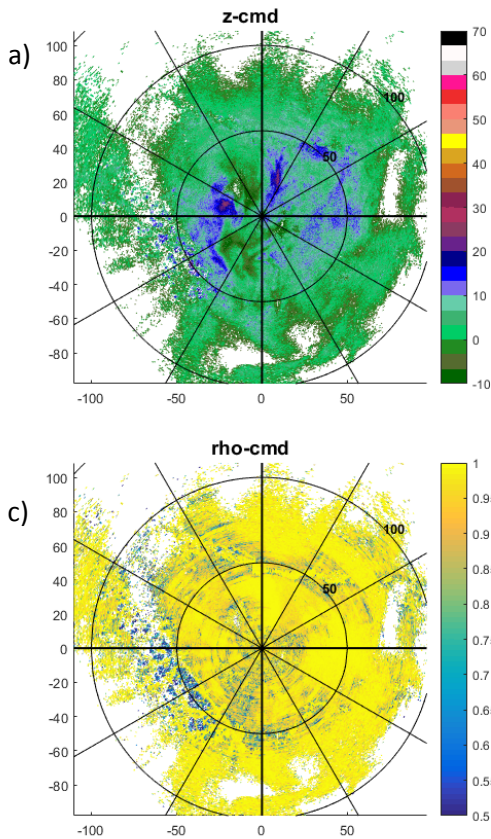


Figure 4: Z (a) and  $\rho_{HV}$  (b) from KRIW with clutter filtering applied to all bins. The data were collected on 24 January 2017 and the elevation angle is 1.5 deg.

### 1.3 Clutter footprint

The high sensitivity of  $\rho_{HV}$ , Zdr and  $\Phi_{DP}$  to low CSR clutter combined with the limited ability of CMD to identify low CSR clutter has resulted in the prevalence of the aptly-named clutter footprint issue. The clutter footprint occurs in conditions of clutter mixed with weather echoes in which CMD has identified the clutter where the CSR is higher than about -5 dB or so and GMAP has been applied so that reasonable estimates of the weather  $\rho_{HV}$ , Zdr and  $\Phi_{DP}$  are recovered. However, at lower values of CSR the clutter is not detected and the  $\rho_{HV}$ , Zdr and  $\Phi_{DP}$  remain contaminated. An example of that is seen in Fig. 5 which shows the Z, Vr and  $\rho_{HV}$  for the data shown in Fig. 3, except the GMAP clutter filter was applied to regions identified as clutter by CMD as shown by the CMD flag field (yellow areas are

identified as clutter). The CMD identifies the strongest clutter, which is then removed by GMAP as seen in the Z field. The  $\rho_{HV}$  was restored to the weather value near 1.0 in regions CMD identified, but the lower CSR regions that were not identified by CMD remain contaminated, resulting in the footprint affect.



conditions that can contaminate  $\rho_{HV}$ ,  $Z_{dr}$  and  $\Phi_{DP}$  the false detection rate would be unacceptably high and the overall performance of the algorithm would be degraded. Thus a new feature field or a new approach for detection of low CSR clutter is needed.

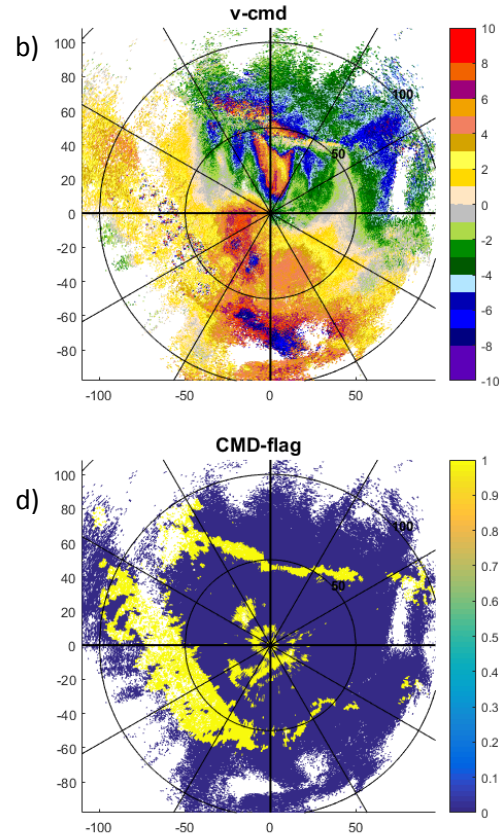


Figure 5: Z (a),  $\rho_{HV}$  (b), Vr (c) from KRIW with clutter filtering applied to bins identified as clutter by CMD shown by the CMD flag field (d). The data were collected on 24 January 2017 and the elevation angle is 1.5 deg.

Figure 5 continued.

### 1.4 Tuning CMD

Hubbert et al. (2015) used a neural network approach to investigate tuning the CMD algorithm with the goal of detecting clutter at lower CSR values and alleviating the clutter footprint issue. It was shown that as the membership functions and weights were modified to increase the probability of detection at very low CSR, the false alarms throughout the rest of the radar domain also increase. It was seen that when CMD was tuned to routinely identify the existence of ground clutter at a CSR values less than about -5 dB, an unacceptably high rate of false detections occurs. This highlights the compromise between false detections and probability of detection that is always a factor in developing and tuning ground clutter detection algorithms. In the case of CMD and its feature fields, in order to detect the very low CSR

### 2 RHOHV-test Method

The proposed method to increase the detection probability of clutter at very low CSR values takes advantage of the fact that application of the GMAP clutter filter repairs  $\rho_{HV}$ . As seen by comparing Figs. 3 and 5 after applying GMAP the  $\rho_{HV}$  was recovered to near 1.0, the intrinsic value of the weather echoes. This is because the  $\rho_{HV}$ , which is the complex correlation of the horizontal and vertical polarized signal within each beam, is generally substantially less than 1.0 for echoes containing more than one echo type - ground clutter and precipitation in this case. Since GMAP removed the ground clutter echo and left only the signal from the snow, the resulting  $\rho_{HV}$  was close to 1.0. This is commonly observed in mixed clutter and weather echoes.

The  $\rho_{HV}$  is often used as a data quality indicator because it is a correlation of the H and V signals and its intrinsic value in weather is commonly close to 1.0 and rarely below 0.7. Therefore a substantial increase in  $\rho_{HV}$  after application of the GMAP generally indicates an improvement in data quality due to the

removal of underlying ground clutter echoes. The observed increase in  $\rho_{HV}$  can also be due to statistical fluctuations, particularly for weather echoes with intrinsic values of  $\rho_{HV}$  less than 1.0, such as melting snow.

The proposed method, dubbed RHOHV-test, is an additional step to the existing CMD algorithm. It requires access to both  $\rho_{HV}$  after application of GMAP on CMD identified clutter regions ( $\rho_{HV}^{CMD}$ ) and  $\rho_{HV}$  after application of GMAP on all bins ( $\rho_{HV}^{AB}$ ). It is recommended to use the GMAP filtered data in regions identified by the RHOHV-test for the variables  $\rho_{HV}$ , Zdr and  $\Phi_{DP}$  and not for the variables Z, Vr and SW. This is due to the variables different sensitivities to low CSR clutter and different susceptibility to clutter filter bias from GMAP described in Sections 1.1 and 1.2.

### 2.1 RHOHV improvement factor

In order to quantify the improvement after the application of GMAP, the  $\rho_{HV}$  improvement factor is computed as,  $\max[0, (1 - \rho_{HV}^{CMD})] / \max[0.01, (1 - \rho_{HV}^{AB})]$ , where  $\rho_{HV}^{CMD}$  and  $\rho_{HV}^{AB}$  are  $\rho_{HV}$  after application of GMAP on bins indicated as clutter by CMD and GMAP applied on all bins, respectively. The maximum functions are applied to avoid negative values of the improvement factor that occur because occasionally estimates of  $\rho_{HV}$  can exceed 1.0 and to avoid dividing by 0.0. The  $\rho_{HV}$  improvement factor for the data shown in Figs. 3 and 5 is shown in Fig. 6. It can be seen that is equal to 1.0 in regions that were previously identified as clutter by CMD. Values of the  $\rho_{HV}$  improvement factor are  $> 1.0$  in regions where low CSR clutter contamination was removed by applying GMAP and values of  $< 1.0$  occur when the GMAP filter reduced  $\rho_{HV}$ , e.g. in the 0 m/s isodop.

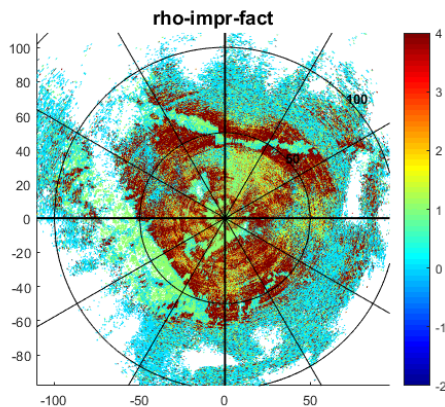


Figure 6:  $\rho_{HV}$  improvement factor for the data shown in Figs 3 and 5.

The  $\rho_{HV}$  improvement factor is a measure of the change of  $\rho_{HV}$  relative to 1.0 that results from using GMAP. A change in  $\rho_{HV}$  improvement factor of 4 means that the  $\rho_{HV}$  after GMAP application is 4 times closer to 1.0 than before. Therefore the absolute

change in  $\rho_{HV}$  differs for a given value of  $\rho_{HV}$  improvement factor depending on how close to 1.0 the unfiltered  $\rho_{HV}$  value is. For example, changing  $\rho_{HV}$  by 0.25 from 0.5 to 0.75 results in a  $\rho_{HV}$  improvement factor of 2.0. In comparison, changing  $\rho_{HV}$  by only 0.05 from 0.9 to 0.95 also results in a  $\rho_{HV}$  improvement factor of 2.0. If GMAP decreases  $\rho_{HV}$  than the  $\rho_{HV}$  improvement factor will be less than 1.0. This happens in the 0 m/s isodop as well as regions of low SNR.

### 2.2 Applying RHOHV-test thresholds

The proposed RHOHV-test method currently has an operating range defined by  $\rho_{HV}^{CMD} < upper\_rho\_thresh$  and  $\rho_{HV}^{AB} > lower\_rho\_thresh$ , where  $upper\_rho\_thresh = 0.98$  and  $lower\_rho\_thresh = 0.5$ . A value of  $\rho_{HV} > 0.98$  is indicative of a highly correlated and well behaved signal such as from rain or snow free of clutter contamination. Therefore to avoid false detections, regions with high  $\rho_{HV}$  prior to GMAP application are not considered. Furthermore it has been shown that there are no hydrometeor echoes with an intrinsic  $\rho_{HV} < 0.5$  (Straka et al., 2000). Therefore if applying GMAP does not recover  $\rho_{HV}$  to greater than 0.5, RHOHV-test is not applied.

For data within the RHOHV-test operating range a threshold ( $rho\_impr\_fact\_thresh$ ) is applied to the  $\rho_{HV}$  improvement factor to determine whether or not to apply GMAP. Therefore, if the  $\rho_{HV}$  improvement factor  $\geq rho\_impr\_fact\_thresh$  GMAP is applied to the data and if the  $\rho_{HV}$  improvement factor  $< rho\_impr\_fact\_thresh$  GMAP is not applied. Currently the value of  $rho\_impr\_fact\_thresh$  is 4.0, meaning that applying GMAP to the data must result in  $\rho_{HV}$  that is 4 times closer to 1.0 than without GMAP in order to be flagged for filtering by RHOHV-test.

### 3 Data

In order to test RHOHV-test on WSR-88D the data sets must contain two data streams: i) the data after CMD processing (i.e. GMAP applied to bins identified as clutter by CMD) and ii) all bins (AB) processing (i.e. GMAP applied to all bins in the radar domain). It is preferable to also have access to the no clutter filter (NCF) data as well for comparison, but these data are not necessary to run RHOHV-test. Since the AB and NCF processing data are not available operationally, the testing required special data collection. This was accomplished by collecting the Archive I, time-series data from special data collections at various WSR-88D sites and for various Volume Coverage Patterns (VCP's). The time-series data were reprocessed using the ROC's playback capability with GMAP configurations: i) NCF, ii) CMD and iii) AB filtering. Finally the three data streams were combined and translated into Matlab Archive 1.9 data files.

The data set includes data from three different radars and four different VCP's: Riverton WY, KRIW VCP 21;

Duluth Minnesota, KDLH VCP 32, KDLH VCP 221; and the Norman testbed KOUN VCP 212.

#### 4 Results

In this section, examples of the results of the proposed RHOHV-test will be presented and compared to the legacy CMD results for each of the radars and VCP's at low elevation angles containing much low CSR clutter contamination. Also presented will be results of RHOHV-test within the melting layer.

##### 4.1 KRIW VCP 21

The first example from Riverton Wyoming is the same case presented in Section 1.1. The data are from 1.5 deg elevation angle during a stratiform snow event providing an excellent example of mixed ground clutter and weather echoes. The unfiltered Z and Vr can be seen in Fig. 2. It can be seen that even at 1.5 deg elevation angle there are strong ground clutter echoes due to ridges in the terrain to the north and southwest of the radar. This is a typical situation for the clutter footprint as demonstrated in Fig. 5.

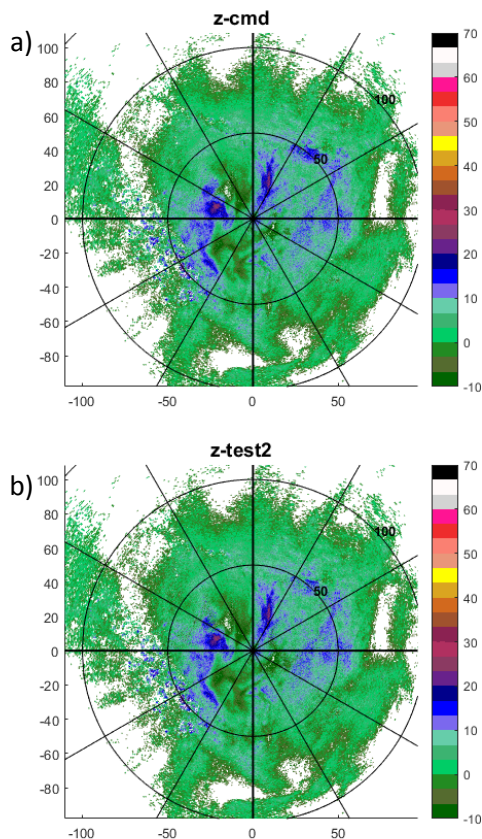


Figure 7: Z after ground clutter filtering following (a) CMD and (b) RHOHV-test. The data were collected by KRIW on 24 January 2017 and the elevation angle is 1.5 deg.

Figure 7 shows the Z field after CMD and RHOHV-test processing. In the case of Z the differences after RHOHV-test are subtle. There are a few range bins that result in the removal of clutter contamination in Z by the application of RHOHV-test near the ridge of strong clutter that was removed by CMD processing to the north of the radar. Also visible in Fig. 7 are several range bins with Z values biased low by after the RHOHV-test. For example at 50 km range and near the 30 deg azimuth spoke and at several azimuth angles at close range. In this case the differences between Z after CMD alone and Z after the RHOHV-test, are quite small, but the benefits of any improvements by removing low CSR clutter are outweighed by the increased clutter filter bias incurred.

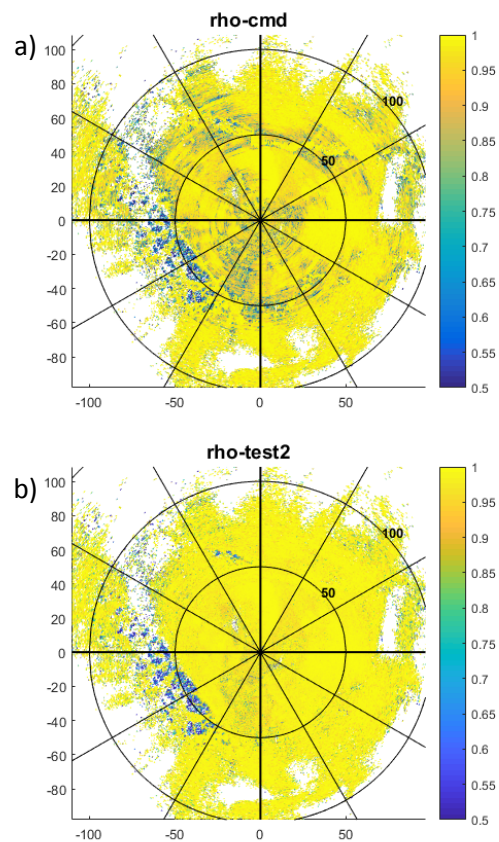


Figure 8: KRIW  $\rho_{HV}$  after ground clutter filtering following (a) CMD and (b) RHOHV-test. The data were collected by KRIW on 24 January 2017 and the elevation angle is 1.5 deg.

The comparison between CMD and RHOHV-test processed  $\rho_{HV}$  are shown in Fig. 8. There are large regions of  $\rho_{HV}$  that are significantly biased by low CSR clutter in the CMD processed data (Fig. 8a). In fact many of the contaminated  $\rho_{HV}$  bins are below 0.9 and 0.8 and as low as 0.5. These low values are not associated with the snow present in the region and will cause errors in the HCA output. After applying the RHOHV-test it can be seen that the vast

majority of the errors due to underlying, low CSR ground clutter are removed (Fig. 8b).

It can be seen that  $\rho_{HV}$  remains biased below the intrinsic  $\rho_{HV}$  value in snow to the southwest of the radar in the region of the strong clutter that was identified by CMD (Fig. 5). In this case the clutter was so strong that there was residual clutter after the filter was applied. This resulted in the  $\rho_{HV}$  not being recovered in this region by application of the clutter filter. It is not possible to recover the precipitation measurements in these areas using the clutter filter.

Another example of data for which the application of GMAP cannot recover  $\rho_{HV}$  occurs where clutter contamination is collocated with the 0 m/s isodop in the precipitation echo. In this case the filter must be applied to remove the clutter, but also causes a bias in the  $\rho_{HV}$  along the 0 m/s isodop. Small examples of this can be seen in Fig. 8 (b) near the radar (e.g. to the southeast between 5 and 10 km in range).

clutter filter bias added to  $\rho_{HV}$  due to applying RHOHV-test processing in the 0 m/s isodop. The filter errors in the 0 m/s isodop can be seen in Fig. 4 (b), which shows  $\rho_{HV}$  with all bins filtering. This must be the case for  $\rho_{HV}$  since the decision whether or not to apply GMAP depends on the improvement of  $\rho_{HV}$  after GMAP is applied. It will, however, be important to ensure no clutter filter bias is imparted onto  $Z_{dr}$  and  $\Phi_{DP}$  in the 0 m/s isodop.

The results of applying the CMD and CMD plus RHOHV-test processing to  $Z_{dr}$  are shown in Fig. 9. Comparing the no clutter filter data (Fig. 9c) it can be seen that applying GMAP to regions designated clutter by CMD (Fig. 9a) removes a large amount of clutter contamination. The clutter footprint and low CSR clutter contamination are not as prevalent in the  $Z_{dr}$  data as for  $\rho_{HV}$ , however there are noticeable contaminated echoes remaining after CMD processing (Fig. 9a). Similar as  $\rho_{HV}$ , the  $Z_{dr}$  contamination due to low CSR clutter remaining after

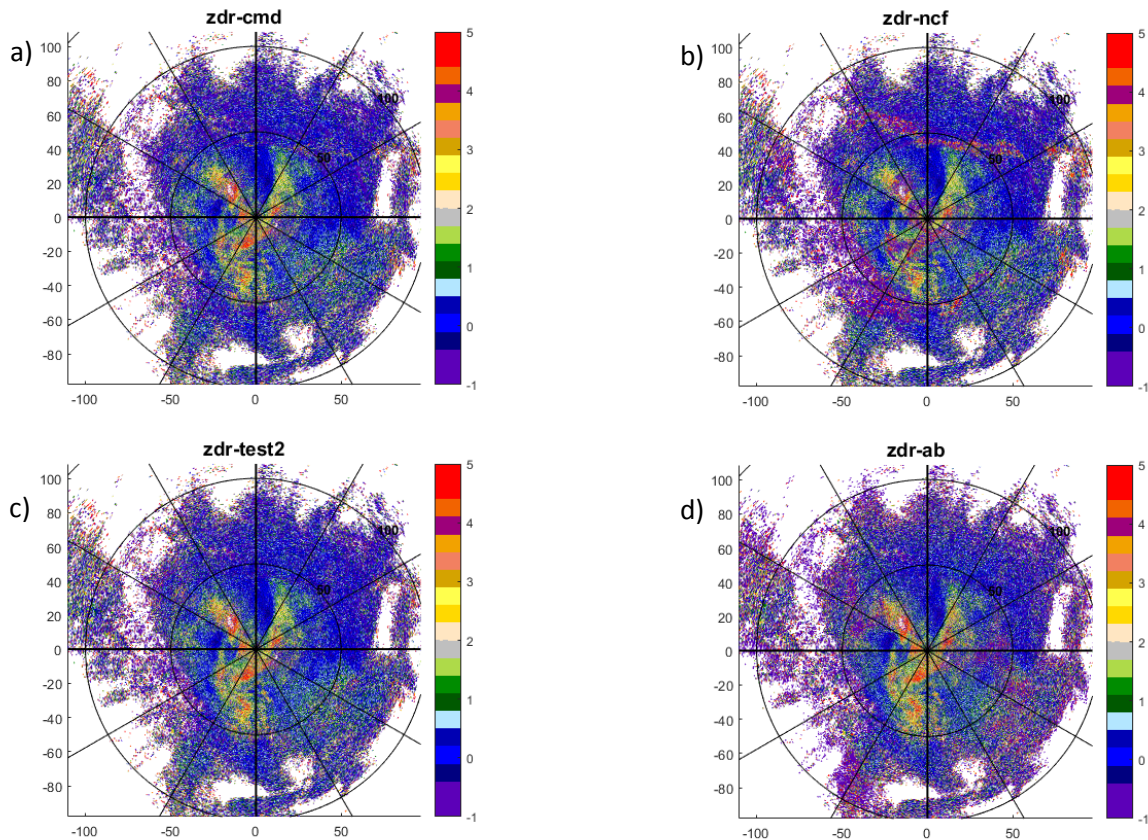


Figure 9:  $Z_{dr}$  after ground clutter filtering following (a) CMD, (b) RHOHV-test.  $Z_{dr}$  with no clutter filtering and all bins filtering are shown in (c) and (d). The data were collected by KRIW on 24 January 2017 and the elevation angle is 1.5 deg.

Figure 9 continued.

CMD are largely removed after RHOHV-test processing (Fig. 9b) resulting in substantially improved data quality.

By design, the RHOHV-test can only increase the  $\rho_{HV}$  values in regions in which the clutter filter can recover the precipitation's  $\rho_{HV}$ . So importantly there is no

The region of strong clutter and clutter filter residue to the southwest of the radar is not recovered for the

same reason as the  $\rho_{HV}$  was not recovered - applying the clutter filter did not recover the precipitation echo.

Importantly the RHOHV-test processed Zdr does not contain additional clutter filter bias in the 0 m/s isodop. This can be seen by comparing the RHOHV-test results to the all bins filtering (Figs. 9b and d). The impact of the clutter filter near the 0 m/s isodop is clearly seen in the all bins filtered data, but none of that bias is visible in the RHOHV-test processed data.

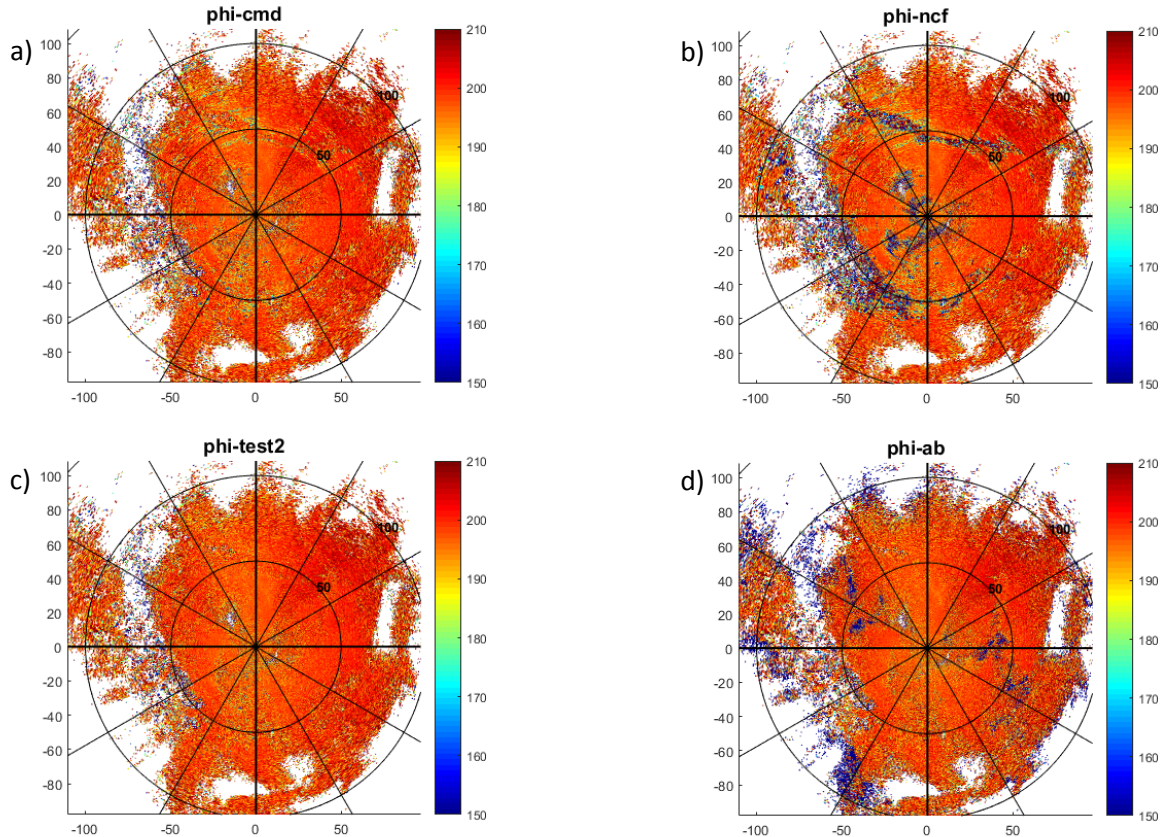


Figure 10:  $\Phi_{DP}$  after ground clutter filtering following (a) CMD and (b) RHOHV-test.  $\Phi_{DP}$  with no clutter filtering and all bins filtering are shown in (c) and (d). The data were collected by KRIW on 24 January 2017 and the elevation angle is 1.5 deg.

The results of applying the CMD and CMD plus RHOHV-test to  $\Phi_{DP}$  are shown in Fig. 10. As for  $\rho_{HV}$  and Zdr, the application of CMD processing (Fig. 10 a) removes a large amount of clutter contamination compared to the unfiltered  $\Phi_{DP}$  (Fig. 10c). The contamination from the low CSR clutter is apparent in the CMD processed data. The majority of this contamination is removed after applying the RHOHV-test (Fig. 10b), resulting in substantially cleaner data. The strong clutter that CMD identified to the southwest of the radar also results in errors in  $\Phi_{DP}$  that cannot be corrected. The clutter filter bias in the 0 m/s isodop evident in the all bins filtered data (Fig

10d) also does not appear in the RHOHV-test processed  $\Phi_{DP}$  data.

#### 4.2 KDLH VCP 32

The next example is from Duluth MN taken on March 16, 2013 at 01:10 UTC. The data are from the 0.5 deg elevation angle. The no clutter filter Z field (Fig. 11 a) shows stratiform snow with ground clutter near the radar and along a ridge to the south of the radar. The

Figure 10 continued

CMD flag (Fig. 11 b) shows that CMD did a good job identifying the strong clutter, which is removed from Z by GMAP (Fig. 11 c). The only clutter filter bias seen is due to clutter overlapping the 0 m/s isodop in Vr (Fig. 11 d), which is not recoverable using a clutter filter.

The  $\rho_{HV}$  field after CMD processing (Fig. 12 a) shows extensive contamination from low CSR ground clutter contamination surrounding the clutter that was identified and removed by CMD processing. After the RHOHV-test processing almost all of the contamination in  $\rho_{HV}$  was removed and the values are restored to near 1.0 as expected in these snow echoes. The only remaining contamination in  $\rho_{HV}$  is in the strong clutter removed by CMD within the 0 m/s isodop, a region that cannot be recovered using GMAP.

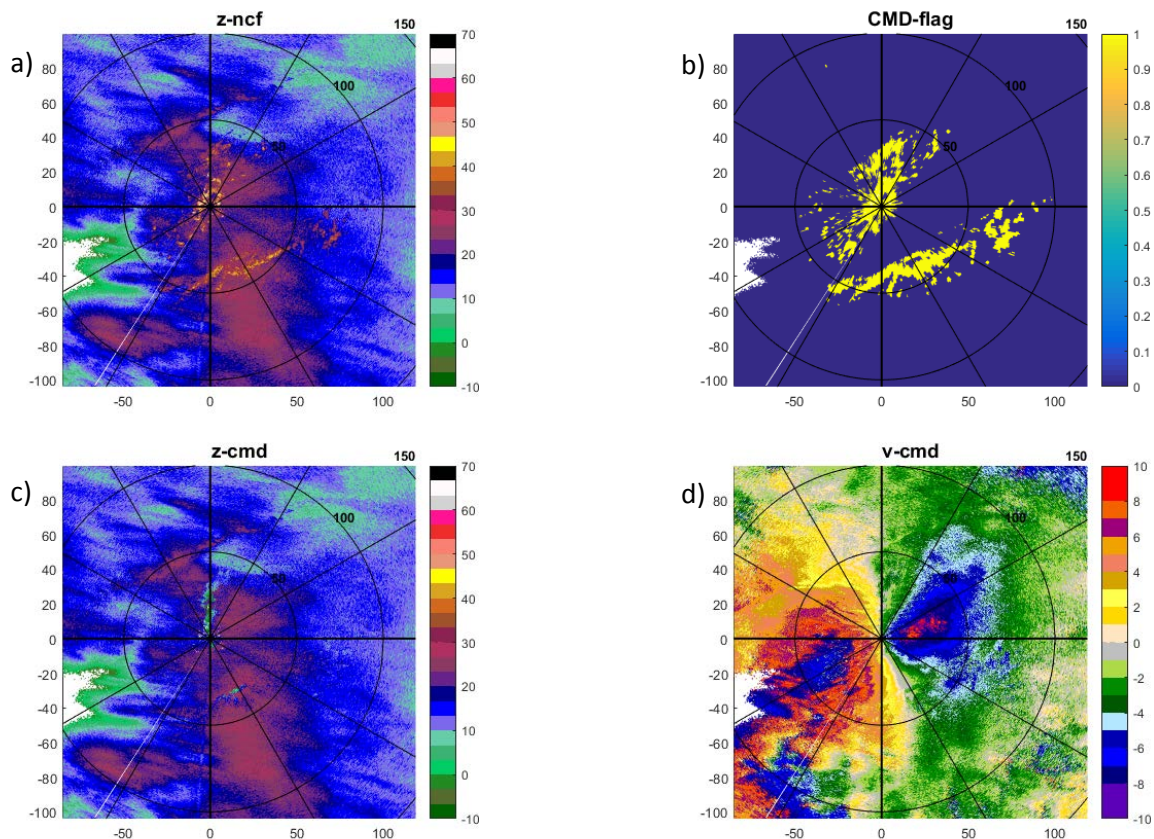


Figure 11: Data from KDLH taken on March 16, 2013 at 01:10 UTC. The data are from the 0.5 deg elevation angle. Shown are Z with no clutter filtering (a), CMD flag (b), Z after CMD processing (c) and Vr after CMD processing (d).

Figure 11 continued.

(KDP), an important variable for hydrometeor classification and precipitation estimation algorithms.

#### 4.3 KDLH VCP 221

The KDLH radar changed the VCP from 32 to 221 in the volume following the time of the results presented in Section 4.2. This allows comparison of the results of RHOHV-test on the different VCP's with very similar conditions. The Z, Vr and CMD flag fields look very similar to the VCP 32. The Z and Vr fields appear slightly noisier with VCP 221 and the CMD flags a slightly larger region as clutter (not shown). The data for this case were collected at 01:21 UTC, about 10 minutes after the VCP 32 example.

The Zdr field after CMD processing (Fig. 13 a) also shows extensive contamination from low CSR ground clutter surrounding the clutter that was identified and removed by CMD processing. The Zdr is biased mainly low by the clutter with many bins well below 0 dB. After the RHOHV-test processing almost all of the contamination in Zdr was removed resulting in substantially improved data quality and Zdr values that are expected in snow and consistent with the uncontaminated echoes in the scan. There is no additional clutter filter bias in the 0 m/s isodop after RHOHV-test processing. Similar as before, the Zdr remains biased where strong clutter was removed from the 0 m/s isodop by CMD processing.

The comparison of CMD and RHOHV-test processed  $\rho_{HV}$  data are shown in Fig. 15. The low CSR clutter bias in  $\rho_{HV}$  that remains after CMD processing stronger and slightly larger in area than for VCP 32 (compare Figs. 12 (a) and 15(a)). Nevertheless, after applying RHOHV-test processing almost all of the low CSR contamination is removed from  $\rho_{HV}$ . As before the  $\rho_{HV}$  cannot be recovered in regions where clutter was removed by CMD processing in the 0 m/s isodop.

Figure 14 shows the results of CMD and RHOHV-test processing for the  $\Phi_{DP}$  field. The low CSR clutter contamination is evident in Fig. 14 (a) in regions similar to that in  $\rho_{HV}$  (Fig. 12 a). After applying RHOHV-test processing, the vast majority of the contamination is removed with no additional clutter filter bias in the 0 m/s isodop. The  $\Phi_{DP}$  resulting from RHOHV-test processing is much smoother and will result in improved specific differential phase shift

The comparison of CMD and RHOHV-test processed Zdr data are shown in Fig. 16. Again the bias in Zdr is stronger for VCP 221 than for VCP 32. The low CSR

clutter bias in Zdr is removed by RHOHV-test processing. The contamination from strong clutter removed from within the 0 m/s isodop remains as before.

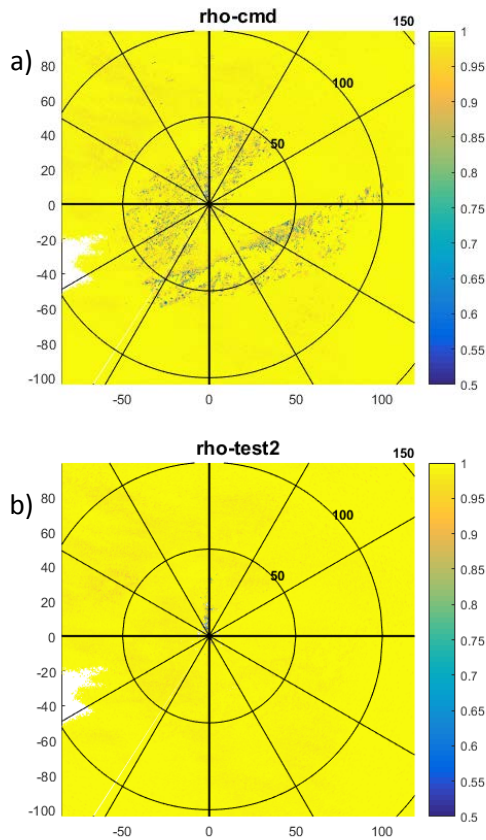


Figure 12:  $\rho_{HV}$  after ground clutter filtering following (a) CMD and (b) RHOHV-test. The data were collected from KDLH using VCP 32 on March 16, 2013 at 01:10 UTC and the data are from the 0.5 deg elevation angle.

The comparison of CMD and RHOHV-test processed  $\Phi_{DP}$  data are shown in Fig. 17. The RHOHV-test processing results in substantially improved data quality with the removal of the majority of clutter contamination without adding additional clutter filter bias in 0 m/s isodop.

The comparison of CMD and RHOHV-test processed  $\Phi_{DP}$  data are shown in Fig. 17. The RHOHV-test processing results in substantially improved data quality with the removal of the majority of clutter contamination without adding additional clutter filter bias in 0 m/s isodop.

The RHOHV-test results on consecutive scans using VCP's 221 and 32 show the method works equally well for both and is robust to the parameters of these 2 VCP's.

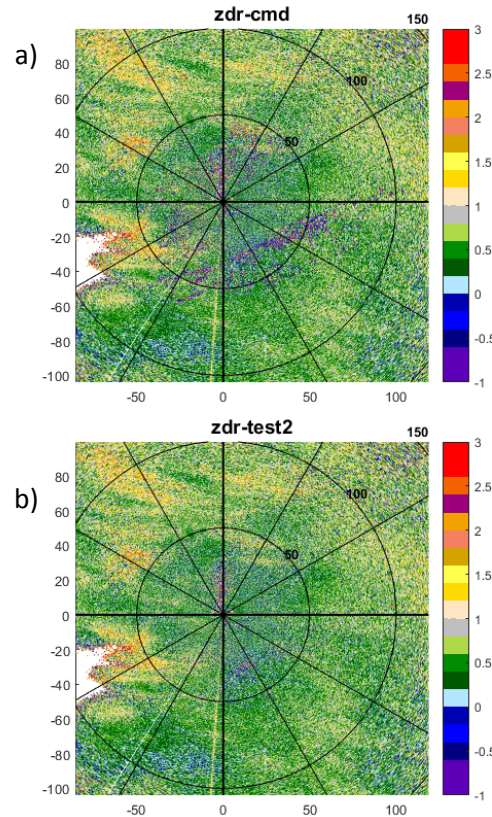
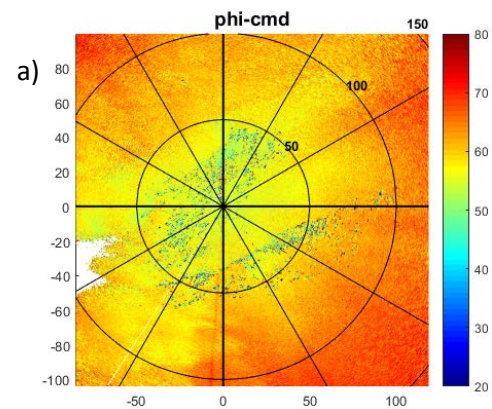


Figure 13: Zdr after ground clutter filtering following (a) CMD and (b) RHOHV-test. The data were collected from KDLH on March 16, 2013 at 01:10 UTC and the data are from the 0.5 deg elevation angle.



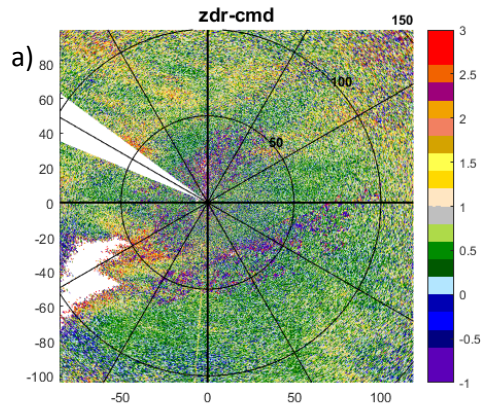
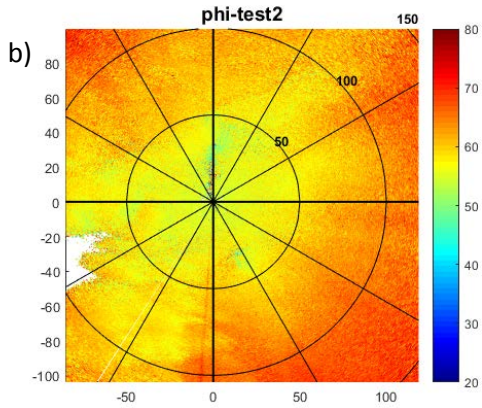


Figure 14:  $\Phi_{DP}$  after ground clutter filtering following (a) CMD and (b) RHOHV-test. The data were collected from KDLH on March 16, 2013 at 01:10 UTC and the data are from the 0.5 deg elevation angle.

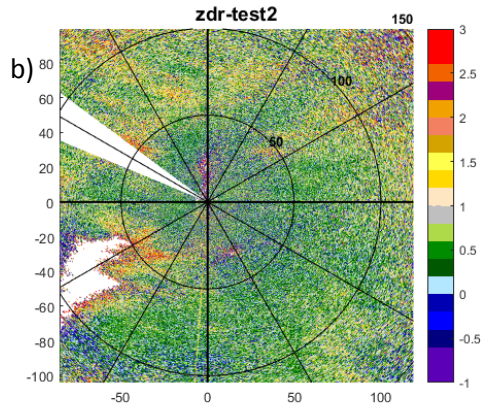
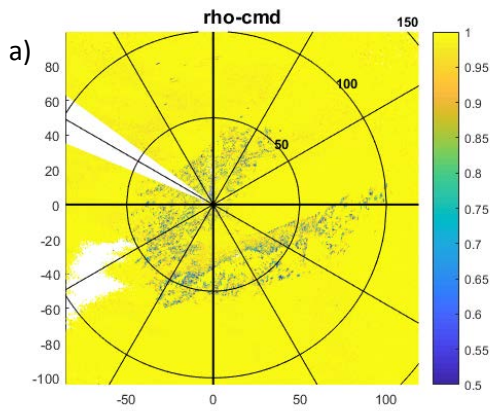


Figure 16:  $Z_{dr}$  after ground clutter filtering following (a) CMD and (b) RHOHV-test. The data were collected from KDLH using VCP 221 on March 16, 2013 at 01:21 UTC and the data are from the 0.5 deg elevation angle.

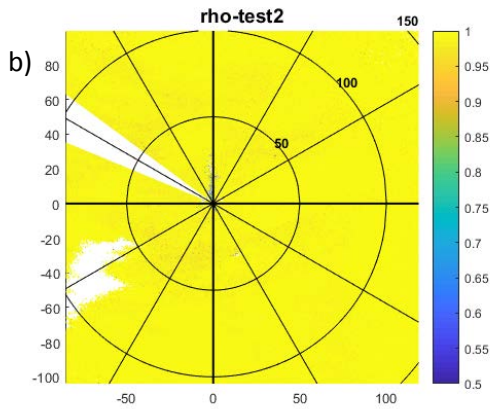


Figure 15:  $\rho_{HV}$  after ground clutter filtering following (a) CMD and (b) RHOHV-test. The data were collected from KDLH using VCP 221 on March 16, 2013 at 01:21 UTC and the data are from the 0.5 deg elevation angle.

#### 4.4 KOUN VCP 212

The next data example comes from the KOUN test bed WSR-88D in Norman OK. This is a case of a convective line approaching KOUN and the radar was

using VCP 212. The no clutter filter Z shows the convective line approaching the radar with light precipitation echoes over the radar and to its east (Fig. 18 a). There is some strong clutter evident close to the radar. The CMD algorithm seems to capture the clutter well (Fig. 18 b) and the CMD processed Z and Vr don't have any noticeable clutter contamination (Figs, 18 c and d).

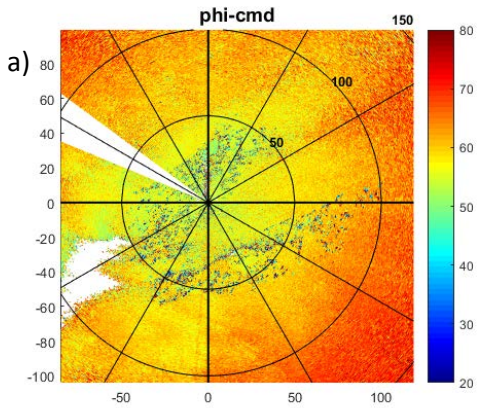


Figure 17 a

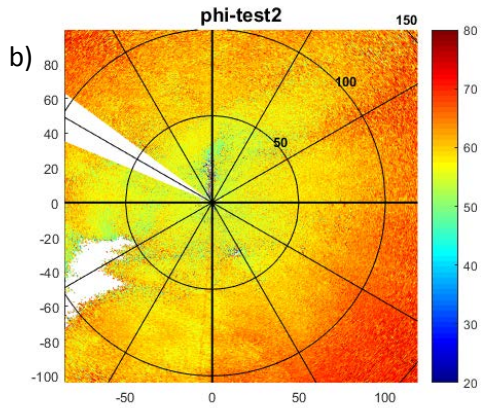


Figure 17:  $\Phi_{DP}$  after ground clutter filtering following (a) CMD and (b) RHOHV-test. The data were collected from KDLH using VCP 221 on March 16, 2013 at 01:21 UTC and the data are from the 0.5 deg elevation angle.

19. After all bins filtering, the  $\rho_{HV}$  still shows a low bias in some of the region contaminated by strong clutter both within and outside of the 0 m/s isodop. The contamination within the 0 m/s isodop is caused by the GMAP filter and the contamination elsewhere is caused by the strong clutter not being completely eliminated. Also on the all bins filtered  $\rho_{HV}$  there are some biases introduced in low SNR regions at the edges of the echo.

After CMD processing the  $\rho_{HV}$  is substantially improved over the NCF case (Fig. 19 a). However a lot of low CSR clutter contamination that went undetected by CMD remains. This low CSR clutter does not have a noticeable impact on Z and Vr, but strongly biases  $\rho_{HV}$ . After applying RHOHV-test processing, the  $\rho_{HV}$  is substantially improved over CMD processing. The majority of the low CSR contamination is removed. There are no additional clutter filter biases introduced by RHOHV-test.

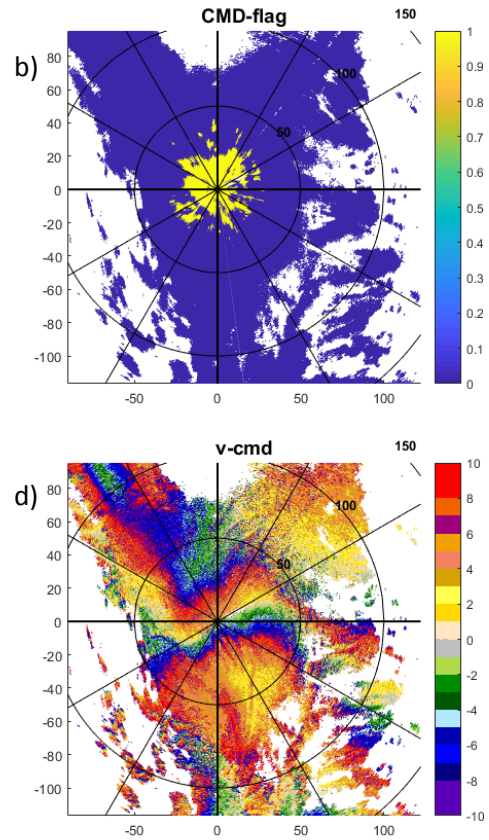
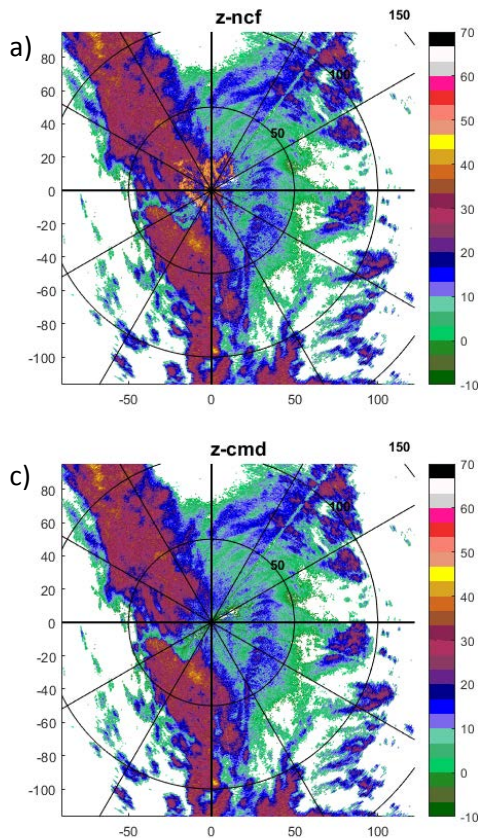


Figure 18: Data from KOUN taken on December 19, 2011 at 23:26 UTC. The data are from the 0.5 deg elevation angle. Shown are Z with no clutter filtering (a), CMD flag (b), Z after CMD processing (c) and Vr after CMD processing (d).

Figure 18 continued

In this case not all of the contamination in  $\rho_{HV}$  in the strong clutter is removed by GMAP, as can be seen by comparing the NCF and all bins filtered data in Fig.

Comparing the CMD processed Zdr (Fig. 21 a) with the RHOHV-test processed Zdr (Fig. 21 b) shows improvement through removal of bias due to low CSR clutter. The impact of the low CSR clutter on Zdr seems to be less pronounced in this case than the previous ones. However there are noticeable biases removed by RHOHV-test processing and there is no

additional clutter filter bias introduced in the 0 m/s isodop.

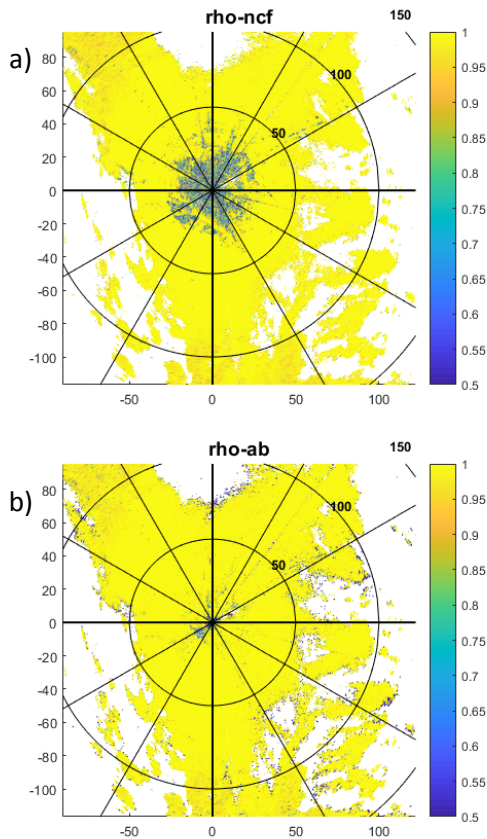


Figure 19:  $\rho_{HV}$  after (a) no ground clutter filtering and (b) filtering on all bins. The data were collected from KOUN using VCP 212 on December 19, 2011 at 23:26 UTC and the data are from the 0.5 deg elevation angle.

The result is similar for  $\Phi_{DP}$ . The low CSR clutter contamination after CMD processing (Fig. 22 a) is removed by RHOHV-test processing (Fig. 22 b) without adding clutter filter bias. As with  $\rho_{HV}$ , the  $\Phi_{DP}$  remains biased in regions in which GMAP cannot recover the data, including strong clutter mixed with 0 m/s Vr weather echo and strong clutter that is not completely removed.

#### 4.5 Melting layer

An important aspect of the RHOHV-test development is to make sure there aren't excessive false detections. False detections are defined here as clutter contamination detected when none exists. Because the RHOHV-test only operates for CMD processed  $\rho_{HV} < 0.98$ , there can't be false detections for weather echoes that have  $\rho_{HV}$  above that range. Since most weather echoes have  $\rho_{HV} > 0.98$ , false detections are limited to echoes in precipitation particles that cause substantial decorrelation, such as melting ice/snow (the brightband), melting graupel,

mixed phase echoes and large hail. False detections are also possible in biological echoes.

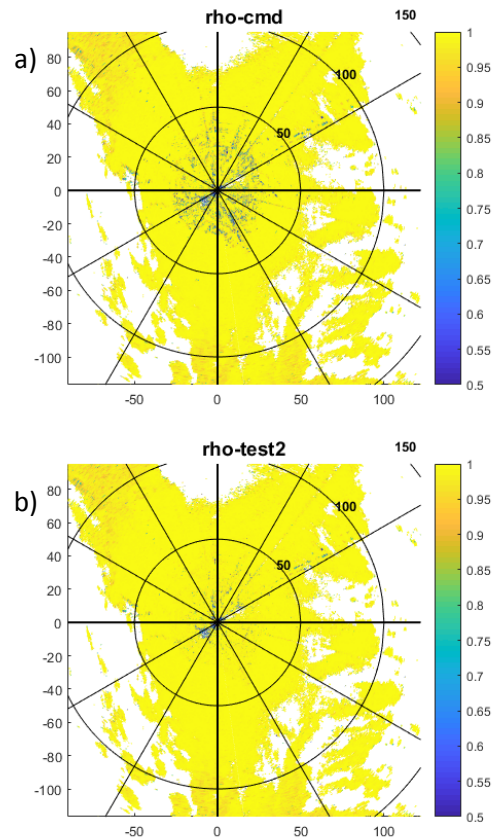


Figure 20:  $\rho_{HV}$  after ground clutter filtering following (a) CMD and (b) RHOHV-test. The data were collected from KOUN using VCP 212 on December 19, 2011 at 23:26 UTC and the data are from the 0.5 deg elevation angle.

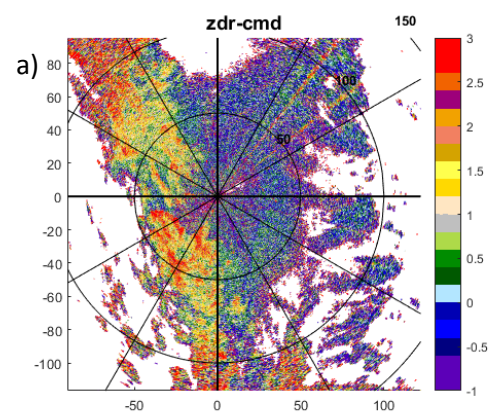


Figure 21 a

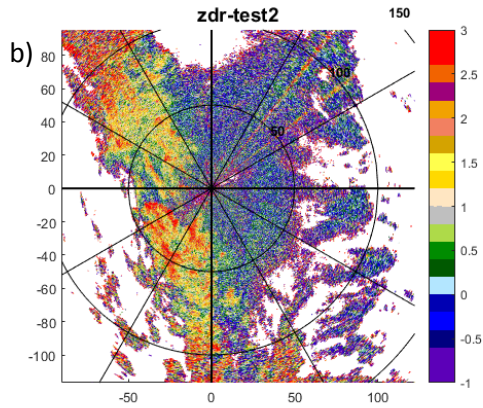


Figure 21: Zdr after ground clutter filtering following (a) CMD and (b) RHOHV-test. The data were collected from KOUN using VCP 212 on December 19, 2011 at 23:26 UTC and the data are from the 0.5 deg elevation angle.

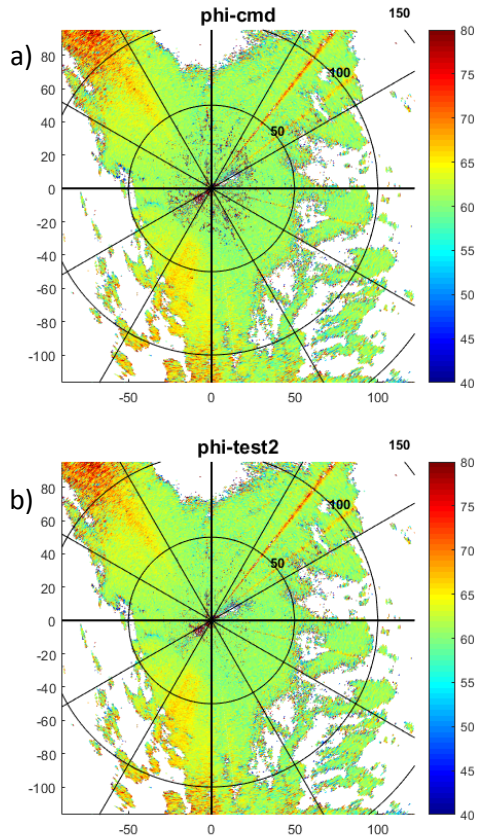


Figure 22:  $\Phi_{DP}$  after ground clutter filtering following (a) CMD and (b) RHOHV-test. The data were collected from KOUN using VCP 212 on December 19, 2011 at 23:26 UTC and the data are from the 0.5 deg elevation angle.

We examine the performance of the RHOHV-test in the melting layer that was present in the KDLH case at 3.5 deg elevation angle. Even at this elevation

angle, there is some clutter contamination, likely from side lobes. Therefore it is impossible to know whether or not clutter detections are correct or incorrect, however if widespread false detections were occurring and inhibiting the detection of the melting layer, it would be noticeable.

Figure 23 shows the CMD processed  $\rho_{HV}$  (a), the combined CMD and RHOHV-test flag (b; a value of 2 indicates CMD detected clutter and a value of 1 indicates RHOHV-test detected clutter), RHOHV-test processed  $\rho_{HV}$  (c) and all bins filtered  $\rho_{HV}$  (d). The melting layer signature is evident by the lower values of  $\rho_{HV}$  centered at a range of about 25 km. It can be seen in the CMD processed  $\rho_{HV}$  that there is some low CSR clutter contamination particularly to the south of the radar. The RHOHV-test flag (b) picks up the low CSR contamination. There is a smattering of clutter identifications in the brightband that may be false detections to the north of the radar. The RHOHV-test processed data clean up the side lobe clutter contamination without imparting any clutter filter bias near the 0 m/s isodop. The melting layer signature is not substantially impacted by RHOHV-test and the overall data quality is improved.

## 5 Summary and Conclusions

This section has discussed the problem of ground clutter mixed with weather echoes, particularly at low CSR. It has been shown that different radar variables have different sensitivity to underlying clutter. The differential variables of  $\rho_{HV}$ , Zdr and  $\Phi_{DP}$  will suffer substantial biases from quite low CSR clutter, as low as -15 dB or below. On the other hand Z and Vr are more robust to underlying clutter. Further, the amount of bias in a given variable can vary substantially for a given CSR level depending on the relative characteristics of the weather and the clutter echoes. These factors show that there is not a single value of CSR that divides data which benefits from clutter filtering and data which should not be filtered.

It was also shown that the Z and Vr are more sensitive to clutter filter bias by GMAP than the differential variables of  $\rho_{HV}$ , Zdr and  $\Phi_{DP}$ . In fact in a region where low CSR clutter biased  $\rho_{HV}$  and did not noticeably bias Z, it was shown that application of GMAP restored  $\rho_{HV}$ , but caused substantial clutter filter bias to Z. This different sensitivity to the application of GMAP combined with the different sensitivity to low CSR clutter of the dual-polarimetric variables and Z and Vr strongly suggest that GMAP be applied in different areas for these variables than for  $\rho_{HV}$ , Zdr and  $\Phi_{DP}$  for improved clutter suppression and clutter filter bias results.

Due to the high sensitivity of  $\rho_{HV}$ , Zdr and  $\Phi_{DP}$  to low CSR clutter, there are often missed detections of clutter contamination that bias these variables in mixed weather and clutter conditions. This has led to the clutter footprint issue. It was previously shown that increasing the probability of detection of low CSR by

tuning the existing CMD membership functions and weights would result in unacceptably high numbers of false detections thereby degrading the overall data quality. Therefore a new approach was sought.

The RHOHV-test method was proposed to increase the detection efficiency of CMD in low CSR contamination of  $\rho_{HV}$ ,  $Z_{dr}$  and  $\Phi_{DP}$ . The method compares the CMD processed  $\rho_{HV}$  to the GMAP filtered  $\rho_{HV}$  and computes the  $\rho_{HV}$  *improvement factor*. The GMAP filtered data are used for radar bins with CMD processed  $\rho_{HV}$  less than 0.98, GMAP filtered  $\rho_{HV}$  greater than 0.5 and a  $\rho_{HV}$  *improvement factor* greater than 4.

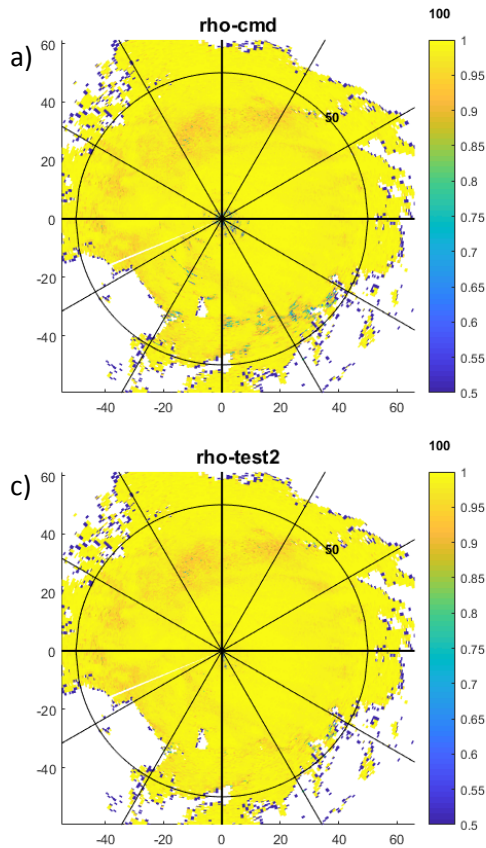


Figure 23: An example from the same data set shown in Section 4.2 but for an elevation angle of 3.5 deg. Shown are (a) CMD processed  $\rho_{HV}$ , (b) the combined CMD and RHOHV-test clutter flag where a value of 2 shows CMD detected clutter and 1 shows RHOHV-test detected clutter, (c) RHOHV-test processed  $\rho_{HV}$  and (d) all bins filtered  $\rho_{HV}$ .

The RHOHV-test was tested on 4 data sets from 3 radars and 4 different VCP's. The results are very encouraging and indicate that the RHOV-test could dramatically improve the data quality of  $\rho_{HV}$ ,  $Z_{dr}$  and  $\Phi_{DP}$  in mixed clutter and weather conditions. Importantly the RHOHV-test does not result in clutter filter bias in  $Z_{dr}$  and  $\Phi_{DP}$  even though it is based on  $\rho_{HV}$ . The false alarms in the melting layer were

minimal and not of consequence. Using the RHOHV-test for filter decisions for  $Z$ ,  $V_r$  and  $SW$  are not recommended. Although limited contamination is removed in  $Z$ ,  $V_r$  and  $SW$  with RHOHV-test there are also substantial clutter filter biases introduced. These variable results are because of the different sensitivity to low CSR and clutter filter bias of  $Z$ ,  $V_r$  and  $SW$  compared to  $\rho_{HV}$ ,  $Z_{dr}$  and  $\Phi_{DP}$ .

The RHOHV-test was shown to be robust to the VCP's available for testing, VCP 32, 212, 221 and 21. The improved  $\rho_{HV}$ ,  $Z_{dr}$  and  $\Phi_{DP}$  using RHOHV-test will have positive impacts on several products. The Hydrometeor ID (HID) commonly misclassifies

Figure 23 continued

regions contaminated with low CSR clutter as biological or unknown. This error in turn will impact the precipitation estimates, which depend on HID.

Based on the results presented in this report, it is recommended that RHOHV-test be implemented for  $\rho_{HV}$ ,  $Z_{dr}$  and  $\Phi_{DP}$  but not for  $Z$ ,  $V_r$  and  $SW$ .